Article

Computer-Aided and AILDE Approaches to Design Novel 4-Hydroxyphenylpyruvate Dioxygenase Inhibitors

Juan Shi †, **Shuang Gao** †, **Jia-Yu Wang, Tong Ye, Ming-Li Yue, Ying Fu** * and **Fei Ye** *

Department of Applied Chemistry, College of Arts and Sciences, Northeast Agricultural University, Harbin 150030, China; shijuan1233@163.com (J.S.); gaoshuang@neau.edu.cn (S.G.); wangjiayu9819@163.com (J.-Y.W.); yetong0812@163.com (T.Y.); yueml@neau.edu.cn (M.-L.Y.)
* Correspondence: fuying@neau.edu.cn (Y.F.); yefei@neau.edu.cn (F.Y.)
† These authors contributed equally to this work.

Abstract: 4-Hydroxyphenylpyruvate dioxygenase (HPPD) is a pivotal enzyme in tocopherol and plastoquinone synthesis and a potential target for novel herbicides. Thirty-five pyridine derivatives were selected to establish a Topomer comparative molecular field analysis (Topomer CoMFA) model to obtain correlation information between HPPD inhibitory activity and the molecular structure. A credible and predictive Topomer CoMFA model was established by "split in two R-groups" cutting methods and fragment combinations ($q^2 = 0.703$, $r^2 = 0.957$, ONC = 6). The established model was used to screen out more active compounds and was optimized through the auto in silico ligand directing evolution (AILDE) platform to obtain potential HPPD inhibitors. Twenty-two new compounds with theoretically good HPPD inhibition were obtained by combining the high-activity contribution substituents in the existing molecules with the R-group search via Topomer search. Molecular docking results revealed that most of the 22 fresh compounds could form stable π-π interactions. The absorption, distribution, metabolism, excretion and toxicity (ADMET) prediction and drug-like properties made 9 compounds potential HPPD inhibitors. Molecular dynamics simulation indicated that Compounds Y12 and Y14 showed good root mean square deviation (RMSD) and root mean square fluctuation (RMSF) values and stability. According to the AILDE online verification, 5 new compounds with potential HPPD inhibition were discovered as HPPD inhibitor candidates. This study provides beneficial insights for subsequent HPPD inhibitor design.

Keywords: HPPD; Topomer CoMFA; molecular docking; molecular dynamics; AILDE

1. Introduction

4-Hydroxyphenylpyruvate dioxygenase (HPPD) is a catalytic enzyme in the synthesis of plastoquinone (PQ) and tocopherol in organisms that converts 4-hydroxyphenylpyruvate (HPPA) to homogentisic acid (HGA) [1–3]. Phytoene will accumulate once the production of PQ is affected. If the HPPD inhibitor interferes with the conversion of HPPA to HGA, it will lead tissue necrosis and albinism symptoms and even plant death [4,5]. Plants in the sun may eventually suffer death with albino symptoms if HPPD inhibitors interfere with the transformation of HPPA to HGA. As a consequence, HPPD becomes a critical latent target for developing novel herbicides [6–9]. HPPD based herbicides play a vital role in rice production by inhibiting the photosynthesis of weeds [10,11]. However, contradictions, such as crop selectivity, weed resistance, herbicide residues, and cost in the development of new herbicides, appear gradually, so it is urgent to explore new green HPPD inhibitors to address these challenges [12,13].

Computer technology promotes drug development and provides theoretical guidance for drug design. Topomer comparative molecular field analysis (Topomer CoMFA), a combination of the initial "Topomer" method and CoMFA technology with 3D-quantitative structure-activity relationship (3D-QSAR) technology and autocomplete regression analysis

can be used to predict the physicochemical properties or biological activity of compounds and screen the database [14,15]. Topomer CoMFA model has been widely used in drug design, such as for Alzheimer's disease, human immunodeficiency virus (HIV), hypercholesterolemia, and breast, lung or renal cell carcinoma [16–19]. The most attractive feature is that Topomer CoMFA provides a relatively objective model because of the wholly automatic process [20,21]. In addition, it facilitates the development of emerging target enzyme inhibitors. The models based on 37 derivatives of 2-phenylquinazolin-4-one predicted novel quinazolinone derivatives as potent tankyrase inhibitors [22–24]. A Topomer CoMFA model was established based on sulfonylurea herbicides, by which 36 new potential inhibitors were obtained by filtration in the ZINC database [25]. Novel antibacterial agents against phytophthora capsici and cucumber peronospora were developed by the Topomer CoMFA model based on carboxylic acid amide fungicides [26]. Fourteen potential human HPPD (*h*HPPD) inhibitors were identified by Topomer CoMFA model screening [27].

Molecular dynamics (MD) simulation is useful for studying protein motion. Drug binding and molecular recognition can be studied by MD simulations [28,29]. Binding free energy identifies the stability of the binding of major residues in protein-ligand interactions, and the molecular mechanical potential energy and solvation free energy during the binding process of the enzyme and the inhibitor have been calculated [30,31]. It revealed that hesperidin, remdesivir, quercetin and sulabiroin-A may be potential natural inhibitors of severe acute respiratory syndrome coronavirus 2 (SARS-CoV-2) [32]. Two potential triketone herbicides have been compared with commercial mesotrione and (2-(aryloxyacetyl) cyclohexane-1,3-dione) by MD simulations, and the screening results are helpful to obtain HPPD inhibitors [33]. The calculation results are more intuitively represented by root mean square deviation (RMSD) and root mean square fluctuation (RMSF) [34].

Hit-to-lead (H2L) is employed to optimize the structure of the compounds, which has been increasingly studied in medicinal chemistry. It has been used against hepatitis B virus (HBV) polycyclic pyridone drugs [35]. In research on antimalarial drugs, two potential drugs were designed via the H_2L method, and the obtained compound activities were verified [36]. Auto in silico ligand directing evolution (AILDE, http://chemyang.ccnu.edu.cn/ccb/server/AILDE/ accessed on 10 February 2021) technology can rapidly identify drug leads in close chemical space [37]. AILDE greatly improves the discovery and synthesis efficiency of potential inhibitors, by which it chemically modifies the molecular fragments of the hit compounds [38].

In this study, a Topomer CoMFA model was built based on 35 pyridine HPPD inhibitors, and potential inhibitors were formed through virtual screening of the more active R-groups in the Bailingwei database (approximately 50,000 fragments). Molecular docking studies further elucidated the interaction between the ligand and receptor. The absorption, distribution, metabolism, excretion and toxicity (ADMET) of the obtained compounds were calculated. The compounds with the best MD simulation verification were submitted to the AILDE server to promote the hit compounds. The filter strategy is shown in Figure 1.
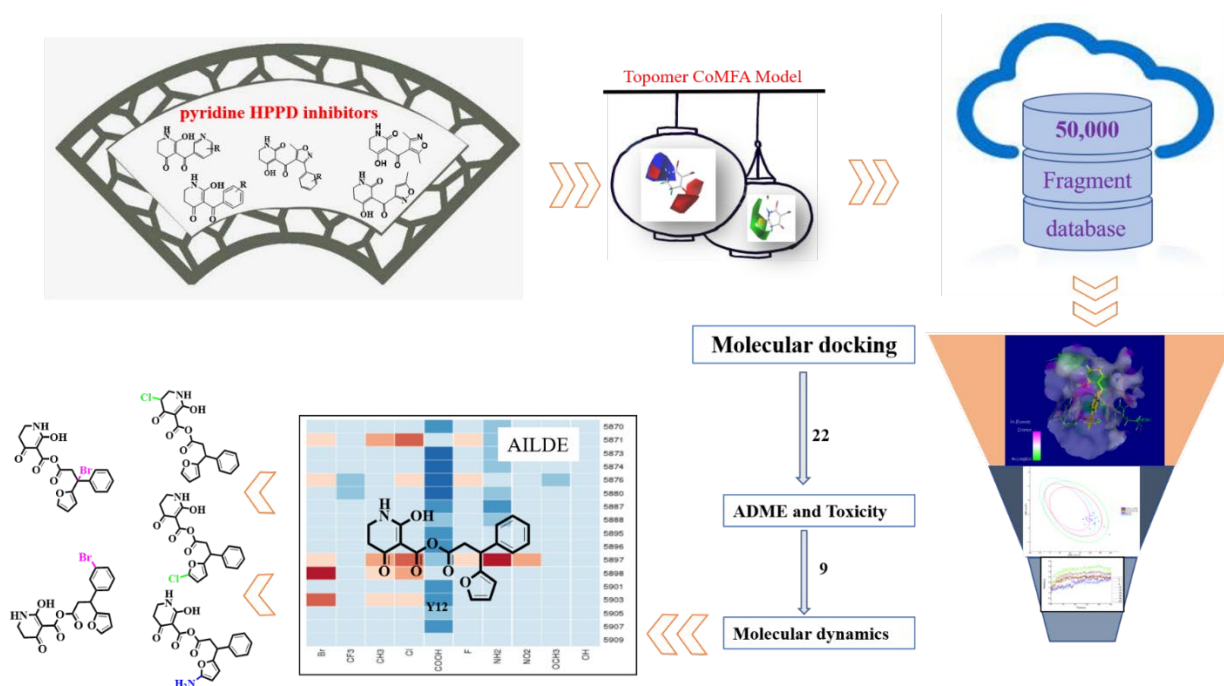
Figure 1. The screening workflow applied to design novel HPPD inhibitors.

2. Results and Discussion

2.1. Topomer CoMFA Analysis

The Topomer CoMFA model statistical results are shown in Table 1.

Table 1. Statistical Results of the Topomer CoMFA.

Cutting Method	q^2	r^2	N	F	SEE	$Intercept$
"split in two R-groups"	0.703	0.957	6	95.338	0.046	4.98

The large q^2 and r^2 ($q^2 = 0.703$, $r^2 = 0.957$) indicated that the prediction was statistically significant. Linear regression plots of experimental and predicted data of HPPD inhibition are shown in Figure 2, showing that the experimental and predicted values were uniformly distributed near the 45° line, which indicated excellent prediction ability. This feature was common in multiple models with screening and prediction capabilities [39–41].
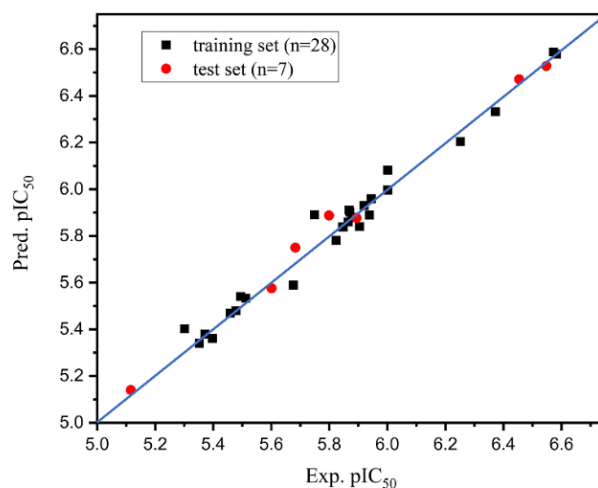
Figure 2. Plot of the experimental and predicted values for training and test set compounds using Topomer CoMFA model.

The steric and electrostatic fields are displayed as contour maps. Figure 3a,b show the steric contour maps of the R^1 and R^2 groups. The green profile enhanced the herbicidal activity by bulky substituents, while the yellow profile enhanced the inhibitory effect by small substituents. A green outline with a large overlap with the plane of the 2-, 3- and 4-positions of the piperidinone of ZD-12 (IC_{50} = 0.325 μM) indicated that the activity can be increased by selecting bulkier substituents at these sites (Figure 3a). As displayed in Figure 3b, a large green outline near the 3-position was also found in the R^2 group. For example, compounds ZD-8 (IC_{50} = 0.283 μM) and ZD-9 (IC_{50} = 0.261 μM) exhibited good activities because of mesyl substituents.
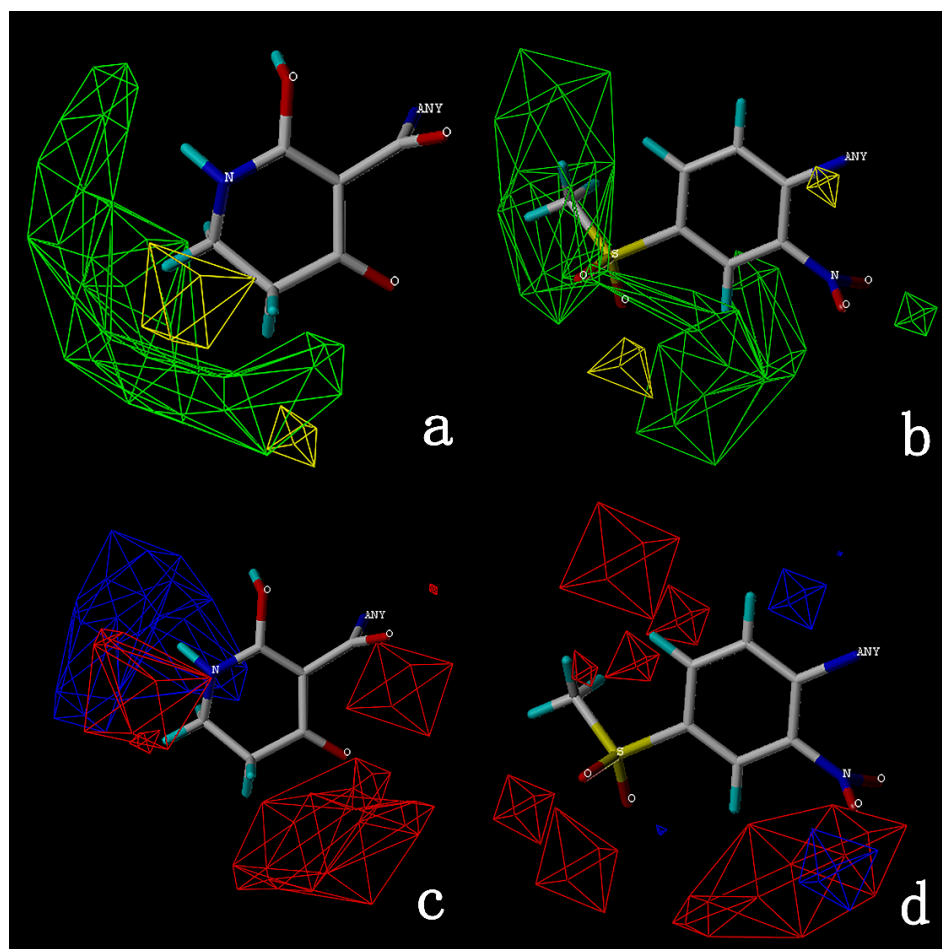
Figure 3. Topomer CoMFA steric (**a,b**) and electrostatic (**c,d**) contour maps based on the R^1 and R^2 groups of the most active ZD-9.

The electrostatic fields are shown in red and blue in the contour maps (Figure 3c,d). For increased weeding activity, red is suitable for negatively charged substituents, and blue isolines are suitable for positively charged substituents. As revealed in Figure 3c, position 4 of the pyridine ring showed a large red outline, and this position should be substituted by a negative charge. The blue outline near the N atom indicated that selecting a positively charged substituent at the N atom site would increase the activity. In Figure 3d, there is a large red outline at the 2 and 3 positions of the phenyl group, indicating that negative charge substitution at this position would increase the activity. For example, ZD-24 (IC_{50} = 1.202 μM) was less active than ZD-27 (IC_{50} = 0.425 μM) due to the methyl being replaced by -Br at the 2-position. For example, the activity of ZD-3 (IC_{50} = 1.365 μM) was worse than ZD-4 (IC_{50} = 0.998 μM) due to methyl being replaced by -CF$_3$ at the 3-position, and the activity of ZD-29 (IC_{50} = 1.589 μM) was worse than ZD-26 (IC_{50} = 0.998 μM) due to

the methyl being replaced by -Cl at the 3-position. A similar effect was observed between compounds ZD-33 (IC$_{50}$ = 7.656 μM) and ZD-32 (IC$_{50}$ = 1.419 μM).

2.2. Topomer Search

Topomer search was employed to screen similar structures or high contribution substituents with HPPD inhibitory activity. The R^2-group model was developed to screen for approximately 50,000 fragments. The hit substituents were ranked according to their value of contribution to activity. Ninety-five new compounds were generated with a contribution value greater than 0.2 as the standard. Then, 64 candidates were obtained by selecting the configuration with the highest score in molecular docking. Finally, 22 molecules were obtained based on the existence of metal coordination bonds. The molecular structures and docking results are shown in Table 2.

Table 2. Structures and -CDOCKER Energy (kcal/mol) of novel designed compounds.
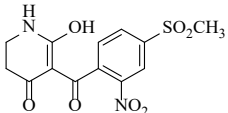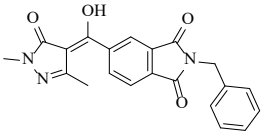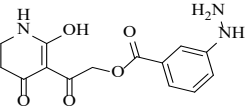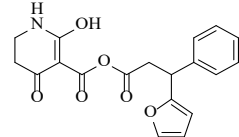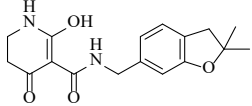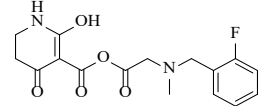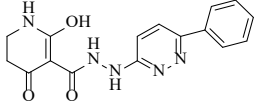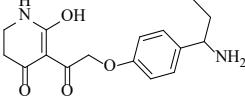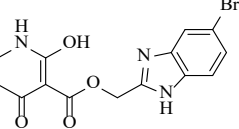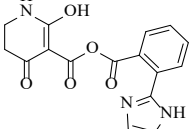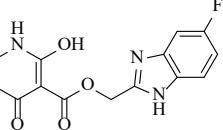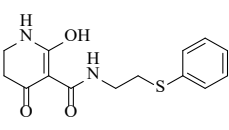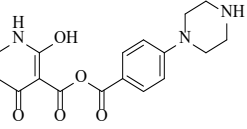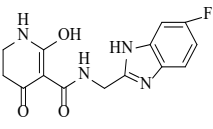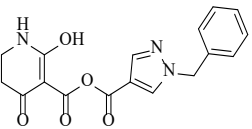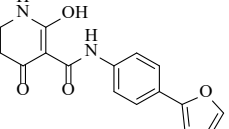
Comp.	Structure	-CDOCKER Energy	Comp.	Structure	-CDOCKER Energy
ZD-9		53.62	Native ligand		51.69
Y1		62.76	Y12		65.51
Y2		51.79	Y13		61.75
Y3		51.66	Y14		69.09
Y4		63.96	Y15		59.92
Y5		54.27	Y16		59.81
Y6		59.48	Y17		58.60
Y7		65.57	Y18		54.28

Comp.	Structure	-CDOCKER Energy	Comp.	Structure	-CDOCKER Energy
Y8		53.29	Y19		59.89
Y9		52.83	Y20		55.52
Y10		58.18	Y21		54.60
Y11		65.12	Y22		60.43

2.3. Molecular Docking Analysis

The CDOCKER program was used to explore the interaction between HPPD (PDB ID: 6JX9) protein residues and ligands [42]. The results were verified by comparing the RMSD between the original ligand and the same interaction site as the original ligand. As shown in Figure 4, the ligand after redocking of the original ligand (red) completely overlapped with the ligand in the complex (cyan) and had exactly the same π-π stacked interactions of Phe381 and Phe424, indicating that the selected protein can be used as a docking model.
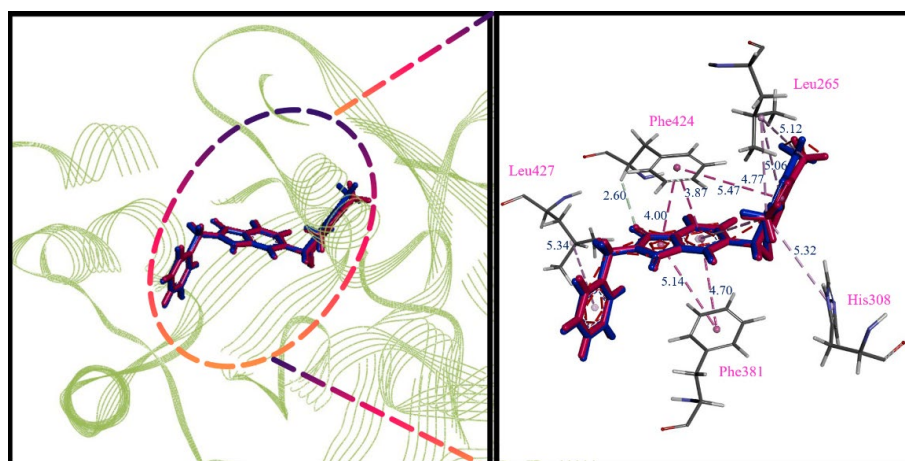

Figure 4. Alignment of the redocked ligands with the native ligand in the crystallographic complex. Redocked ligand is cyan, the native ligand is red. Green is the distance of the interaction (Å).

Subsequently, all the newly designed molecules and the most active ZD-9 were docked into 6JX9, and the -CDOCKER energy is shown in Table 2. The -CDOCKER energies were all above that of the native ligand (51.69 kcal/mol), which confirmed that the designed compounds exhibited better docking results coincidence than the native ligand. The -CDOCKER energy (65.51 kcal/mol) of Y12 was greater than that of the native ligand. The π-π stacked interactions between Y12 and Phe392 may be the reason for the -CDOCKER energies of Y12 compared with the native ligand. The most active compound, ZD-9, was

selected as the template for detailed description. Two compounds, Y12 and Y14, with the best -CDOCKER energy were selected to analyze the binding mode at the active pocket.

As shown in Figure 5a, ZD-9 was fully embedded into the active pocket. The hydrogen atom of the imino formed hydrogen bonds with the oxygen atoms of Ser267; the two carbonyls produced metal coordination bonded with cobalt ions; and the benzene rings formed π-π interactions with Phe381 and Phe424. This was consistent with the docking results reported earlier [43]. Figure 5b showed that the π-π interaction of the pyridine ring of Compound Y12 was similar to that of ZD-9. Moreover, Phe381 also formed a π-π interaction with the furan ring of Compound Y12, and Gln379 formed hydrogen bonds with carbonyl outside the pyridine ring, which made Compound Y12 binding more stable than ZD-9. Compound Y14 was also well inserted into the active site of the protein, as shown in Figure 5c. It also interacted with amino acids Phe381 and Phe424, similar to ZD-9, and the necessary metal coordination bonds and hydrogen bonds also exist.
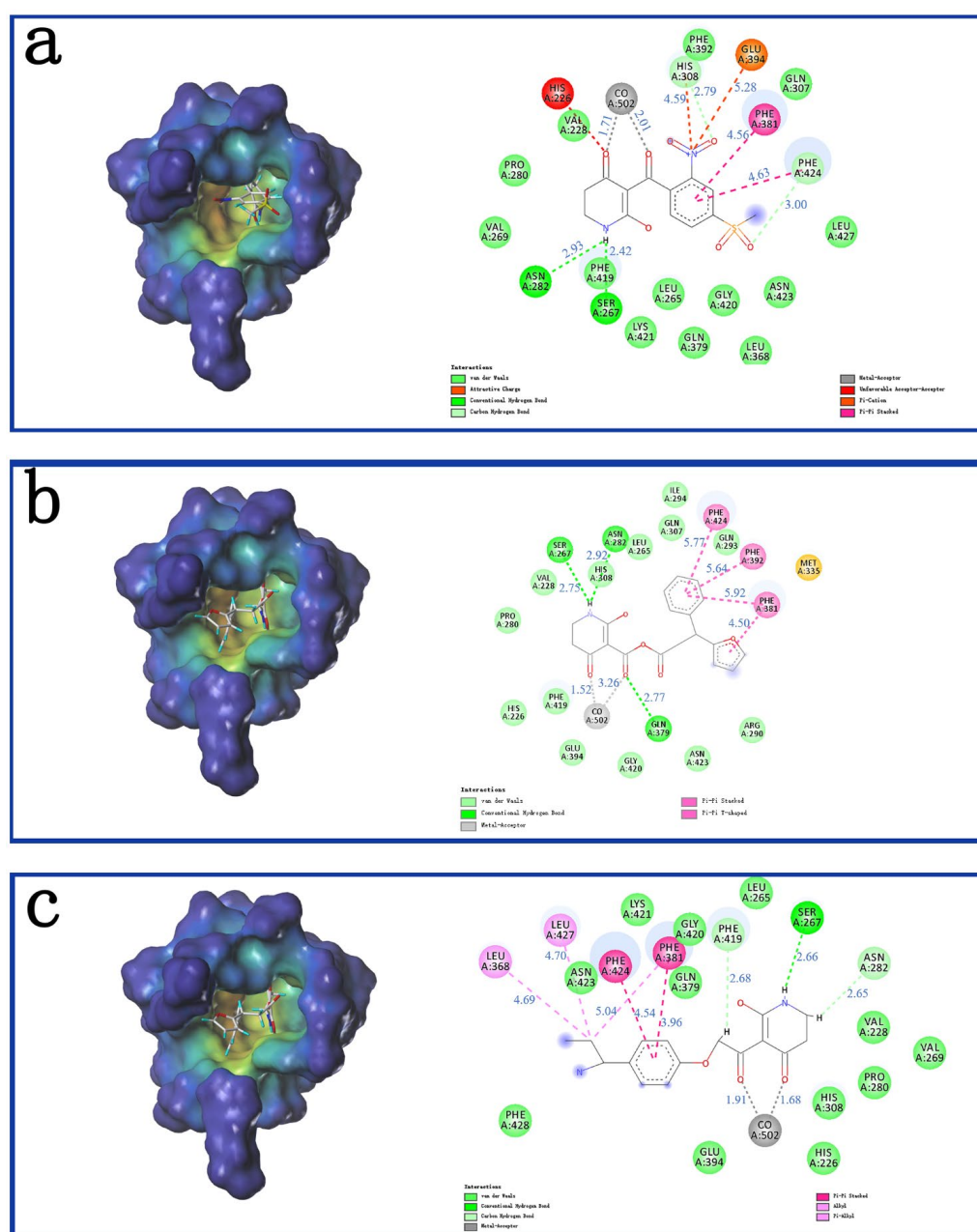

Figure 5. The receptor-ligand interaction of ZD-9 (**a**), Y12 (**b**) and Y14 (**c**) in the HPPD active site. Blue is the distance of the interaction (Å).

2.4. ADMET Prediction

Then, the 22 newly designed compounds were subjected to ADME analysis. The molecules that exist in the 99% confidence interval of the blood–brain barrier permeability model and the 99% confidence interval of the human intestinal absorption model were selected as the hit compounds, and 18 of them showed ADME properties in the acceptable range (Figure 6). The bayesian score of compounds in the hepatotoxic were less than −0.41 (Table 3). Therefore, these newly designed molecules had excellent physical and chemical properties, low toxicity and good crop protection.
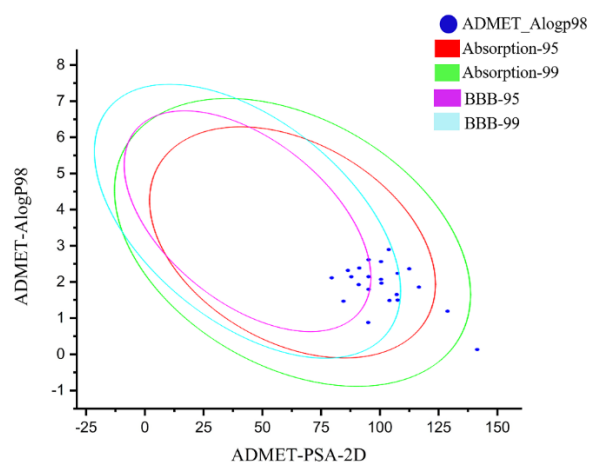

Figure 6. ADMET prediction for all designed compounds.

Table 3. The ADME predictions of compounds.

Comp.	Solubility Level	Hepatotoxic	CYP2D6_Applicability
Y1	3	−2.52	13.33
Y2	3	−0.71	18.64
Y3	3	−0.99	15.80
Y4	3	−1.57	14.34
Y5	3	−0.46	13.20
Y6	3	−0.89	12.68
Y7	3	−2.85	15.91
Y8	3	−2.03	14.99
Y9	3	−0.43	17.18
Y10	3	−4.56	11.17
Y11	4	−3.20	12.81
Y12	3	−1.68	11.07
Y13	3	−2.06	13.78
Y14	3	−3.28	13.22
Y15	3	0.84	15.14
Y16	4	−0.73	13.56
Y17	3	−2.25	14.67
Y18	3	−3.45	13.58
Y19	4	−1.24	15.39
Y20	4	−0.09	19.39
Y21	4	−1.01	18.93
Y22	3	−3.68	13.27

Solubility Level: Categorical solubility level. 2: Yes, low; 3: Yes, good; 4: Yes, great. Hepatotoxic: <−0.41: nontoxic; >−0.41: toxic.

The toxicity prediction (extensible model of ADME) results indicated that the reference compound ZD-9 is non-mutagenic, noncarcinogenic and degradable. Only nine of the newly designed compounds met the criteria of non-mutagenicity, non-carcinogenicity and degradability (Table 4).

Table 4. Toxicity prediction of the new compounds and reference compounds.

Comp.	Degradability	Mutagenicity	Carcinogenicity
ZD-9	√	×	×
Y1	×	×	×
Y2	√	×	×
Y3	×	√	×
Y4	×	×	√
Y5	×	√	×
Y6	×	×	×
Y7	√	×	×
Y8	×	√	×
Y9	√	×	×
Y10	√	×	×
Y11	×	×	×
Y12	√	×	×
Y13	×	×	×
Y14	√	×	×
Y15	√	×	×
Y16	×	×	×
Y17	×	√	×
Y18	√	×	×
Y19	√	×	×
Y20	√	×	×
Y21	×	×	×
Y22	×	×	×

2.5. MD Simulations

To further determine the accuracy of the docking procedure, the native ligand and the redocked ligand were simulated by MD simulation. The active pocket of the 5 Å residue around the ligand stabilizes after 10 ns, and the redocked ligand was below the native ligand, indicating that the redocking procedure will be more stable (Figure 7a). The skeleton Cα atoms of redocked ligand and native ligand fluctuate at about the same trend after 7.5 ns (Figure 7b). The heavy atoms of the native ligand-receptor were 2.5 ns ahead of the redocked ligand-acceptor (Figure 7c). The native ligand and the redocked ligand proved the docking procedure was correct under similar fluctuations and stability.

To further determine the accuracy of the hit, 9 compounds screened by ADMET were simulated by MD simulation to determine whether the binding of the HPPD-ligand complex was stable. The overall stability of the system was evaluated by monitoring the RMSD of skeleton atoms. Skeleton Cα atoms of proteins, active pockets of 5 Å residues around ligands and heavy atoms of ligands-receptor were simulated in 50 ns. The side chain flexibility was generally higher than that of the backbone atoms; therefore, the RMSD of the main chain is a crucial indicator of system stability.

Figure 8a showed that the residues within 5 Å around the protein active pocket ligand stabilized after 20 ns, and then, the RMSD value remained unchanged. In Figure 8b, the HPPD-Y12 and HPPD-Y14 complexes fluctuated in a small range at the beginning and gradually reached equilibrium after 5 ns of simulation. The RMSD values of the remaining seven HPPD complexes were stable after 10 ns. The stable RMSD values of complexes Y12 (1.0 Å) and Y14 (0.5 Å) were significantly lower than those of the other seven compounds, indicating that these two complexes were more stable. The heavy atoms of the ligands-receptor tended to balance after 10 ns, and the RMSD value remained stable (Figure 8c).
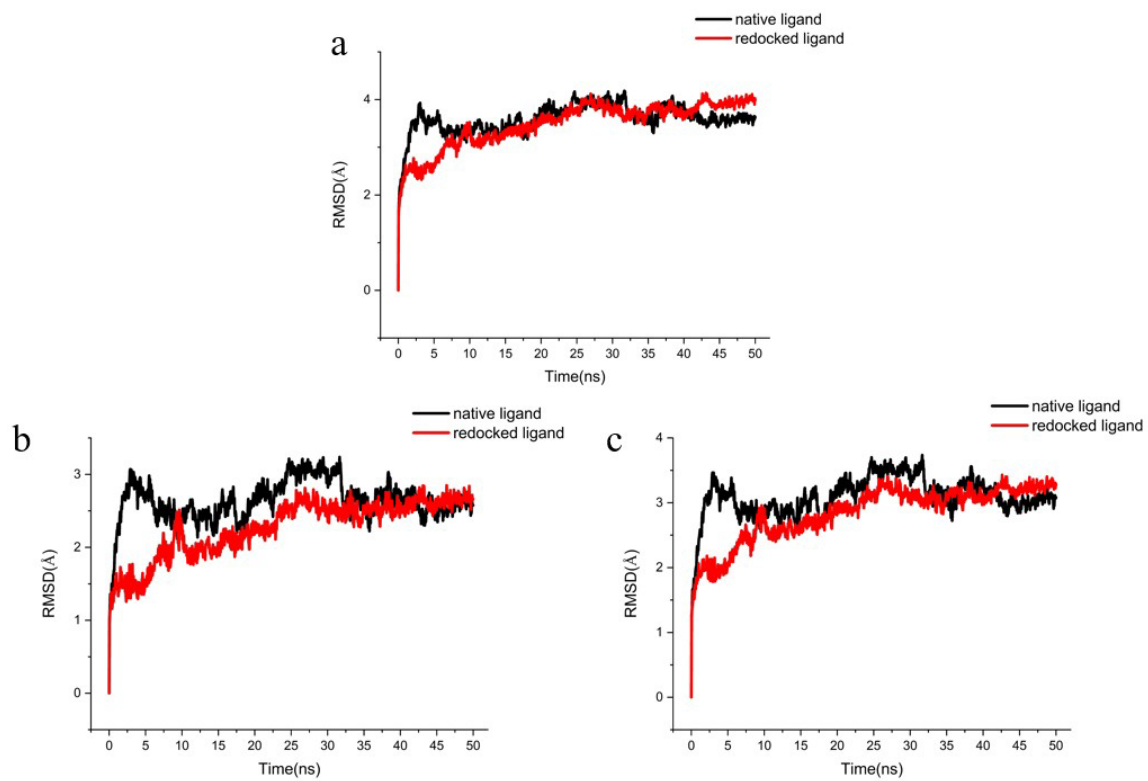
Figure 7. The RMSD trajectories of the redocked ligands with the native ligand during 50 ns simulations. (**a**) The protein active pocket with residues of 5 Å around ligand, (**b**) backbone Cα atoms and (**c**) heavy atoms of ligand-receptor.
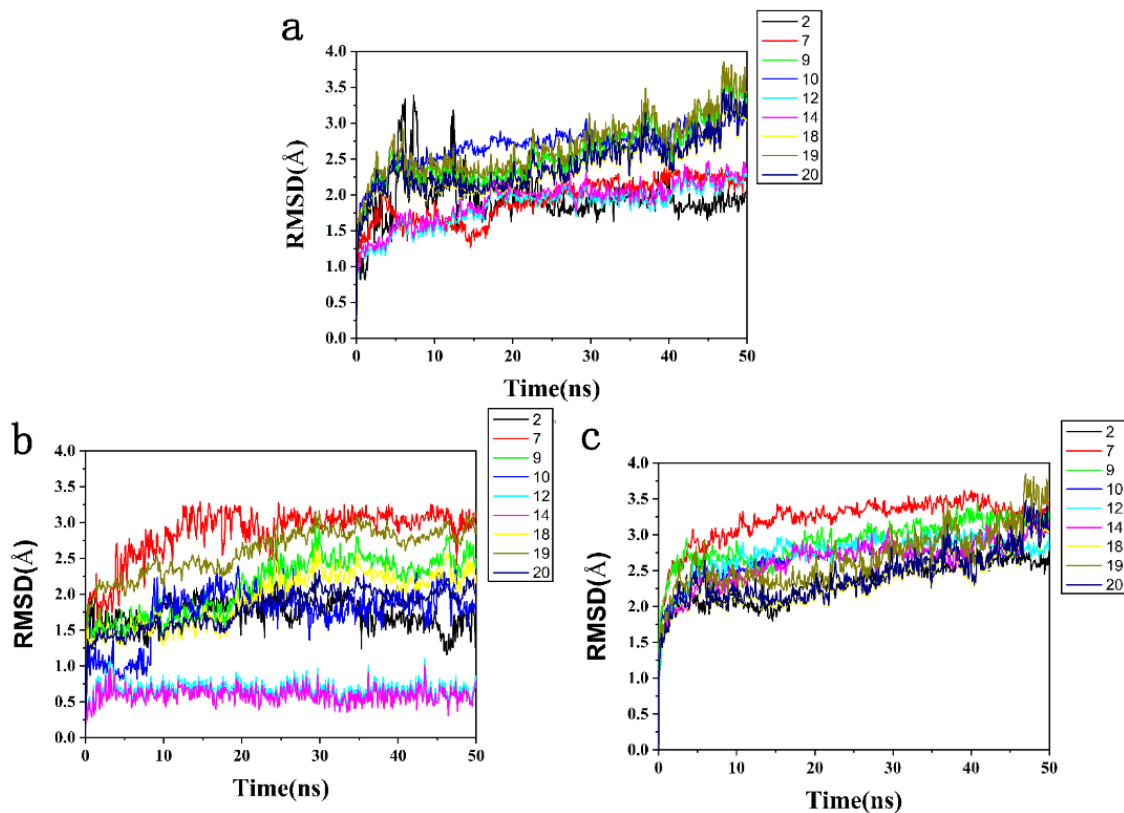

Figure 8. The RMSD trajectories of all systems during 50 ns simulations. (**a**) The protein active pocket with residues of 5 Å around ligand, (**b**) backbone Cα atoms and (**c**) heavy atoms of ligand-receptor.

A lower RMSD of the docking complexes was a good indicator of system stability. The structural fluctuations of the HPPD-Y12 and HPPD-Y14 systems were relatively lower than those of the other molecules. These results suggested that Y12 and Y14 exhibited relatively favorable binding affinity with HPPD.

In addition, the results of RMSF are shown in Figure 9. The peak represents the region where the protein fluctuates the most during the simulation. Due to hydrogen bonding between Asn282, Ser267 and ligands, structural flexibility was significantly increased in the residue index of 250–300, and the residue index of 350–400 was the π-π stacked interactions on account of Phe381 (Figure 9a). It was generally observed that the tail (N-terminal and C-terminal) fluctuated more than other parts of the protein. Secondary structural elements such as alpha helical and beta strands are generally less volatile than unstructured parts of proteins than loop regions. This phenomenon was also seen in (Figure 9b,c). All compounds characterized local changes in the protein chain and simulated fluctuations in RMSF values corresponding to the terminal portion which were higher than the intermediate portion.
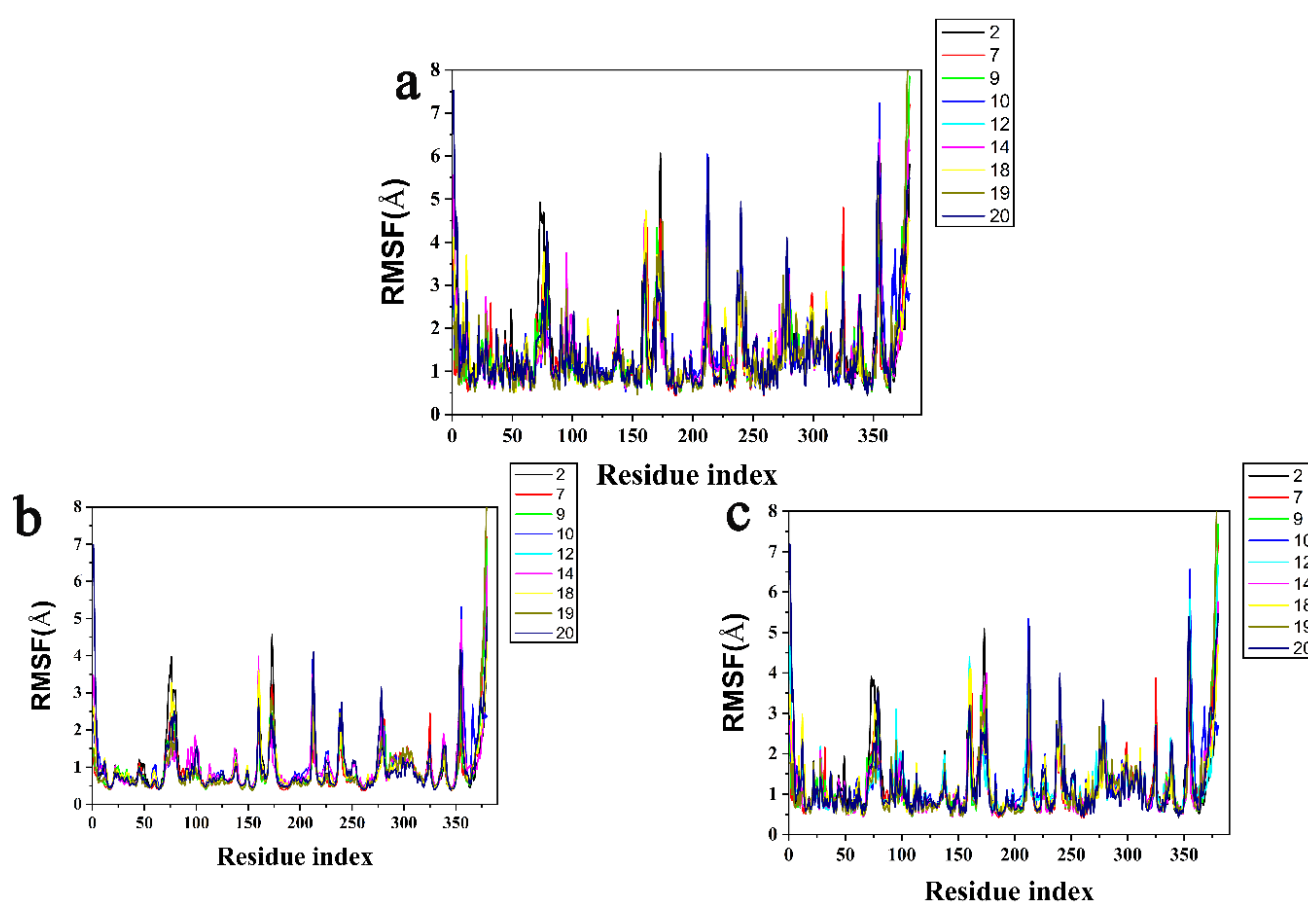
Figure 9. Protein RMSF for (**a**) the protein active pocket with residues of 5 Å around (**b**) Cα atoms and (**c**) heavy atoms.

2.6. AILDE Optimized Hit Compounds and Physicochemical Properties

The AILDE method was the ligand substitution scanning mutagenesis calculation method, one of the strategies used in H2L optimization in agricultural chemical design [44]. Compound Y12 was submitted to the online server for AILDE verification because it exhibited the best molecular docking and MD simulation verification results. The activities of the compounds were input into the AILDE server, and computation substituent optimization was performed by replacing the hydrogen number in the structure (Figure 10a). The results of the heat map in Figure 10b showed that the redder the compound was, the better the activity was. For example, if the hydrogen at position 5871 was replaced by chlorine, the hydrogen at position 5897 was replaced by chlorine or amino, or if the hydrogen at

positions 5898 and 5903 were replaced by bromine, more active compounds would be obtained. The overall results based on the corresponding substituents are illustrated in the histogram in Figure 10c.
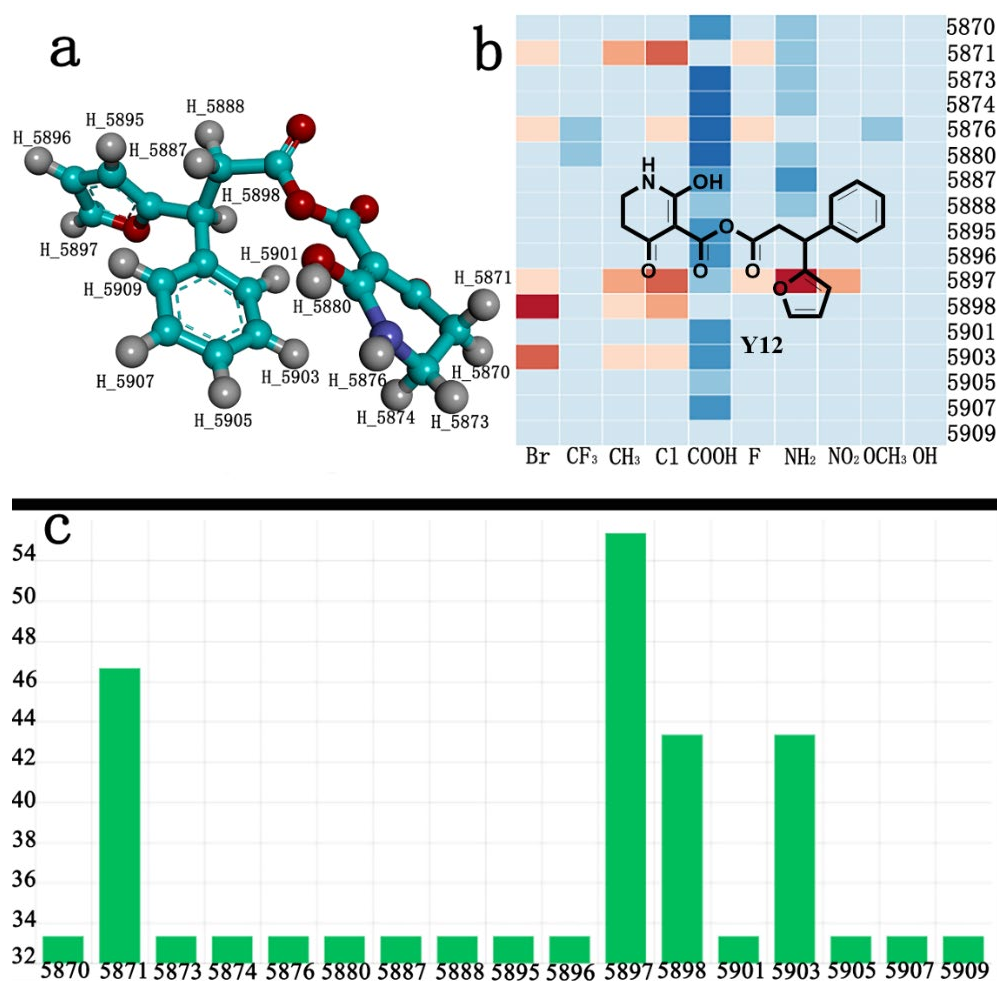

Figure 10. (**a**) Hydrogen serial numbers; (**b**) Heat map showing the relationship matrix between the substituent positions and substituents (darker red colors indicate compounds with better activities); (**c**) Histogram illustrating the overall result based on substituent positions, which helps to elucidate which positions possess the most potential for substitution (X: Hydrogen number, Y: Score).

The greatest potential transformation was shown at positions 5871, 5897, 5898, and 5903. Then, five compounds were obtained after screening (Table 5). If the substitution of the hydrogen atom at position 5897 was by an amino group, the ΔG value was the smallest; thus, the compound had priority. In summary, the use of AILDE will improve the efficiency of initial drug discovery, which also provides favorable guidance for subsequent synthesis work.

The amount of HBA, HBD and AR in the compound is positively correlated with biological activity [45,46]. It is worth noting that the number of HBA and HBD of S3 is slightly higher than that of Y12 (Table 6). The electronegativities of the five compounds obtained are very similar, and their predicted pKa values are less than 6.0, which are even lower than that of Y12 without optimization. Weak acidity and low Log *p* are conducive to the spread and absorption of plants. Based on the physical and chemical properties, the optimized process is beneficial for obtaining new HPPD inhibitors.

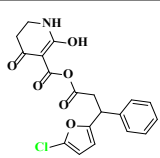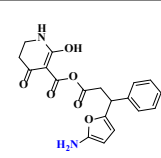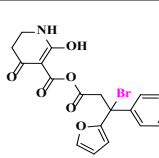**Table 5.** Screening result for 5 compounds.
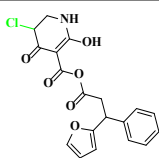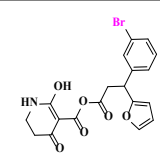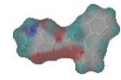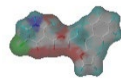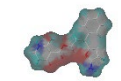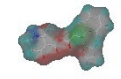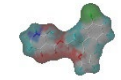
Comp.	S1	S2	S3	S4	S5
Structure					
Hydrogen Number	5871	5897	5897	5898	5903
ΔG (kcal/mol)	−1.23	−0.98	−1.87	−1.53	−1.23
ΔH (kcal/mol)	−1.61	−1.27	−2.24	−1.72	−1.25
$-T\Delta S$ (kcal/mol)	0.38	0.29	0.37	0.19	0.03

Table 6. Screening result for 5 compounds.

Comp.	Log p [a]	pKa [a]	M_W [a]	HBA [a]	HBD [a]	RB [a]	SA [a]	Electronegativity [b]
Y12	2.11	5.7	355.34	6	2	7	342.81	
S1	2.66	5.6	389.79	6	2	7	361.58	
S2	2.57	5.6	389.39	6	2	7	362.88	
S3	1.49	5.6	370.36	7	3	7	358.47	
S4	2.86	5.6	434.24	6	2	7	370.40	
S5	2.86	5.6	434.24	6	2	7	368.19	

Notes: [a] DS for predicting Log p, pKa, molecular weight (M_W), hydrogen bond acceptor (HBA) and donor (HBD), rotatable bonds (RB) and surface area (SA); [b] SYBYL for predicting electronegativity.

3. Methods and Materials

3.1. Information Collection

The structures and bioactivities of the 35 pyridine derivatives employed in this experiment were derived from our laboratory [43]. These pyridine derivatives are different in aromatic subunit. The collection of derived compounds contained 28 compounds as training sets and 7 compounds as test sets. Topomer CoMFA model was constructed with these compounds, and the predictive ability of the model was tested. The bioactivity and chemical structure are reported using the pIC$_{50}$ data in Table 7.

The Sketch module in SYBYL was used to construct molecular structures. All compounds were perfected using a Tripos force field and gradient descent with an energy charge of 0.005 kcal/mol. Gasteiger–Huckel adds partial charges to all compounds. The maximum iteration coefficient was selected as 1000, and the other parameters default to SYBYL. Energy minimization was optimized for all molecules. The minimum energy conformation of the best active compound ZD-9 (6-hydroxy-5-(4-(methylsulfonyl)-2-nitrobenzoyl)-2,3-dihydropyridin-4(1H)-one) was selected as the template compound.

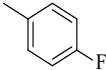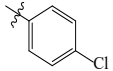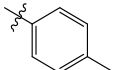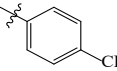**Table 7.** Pyridine derivatives used for the Topomer CoMFA analysis.
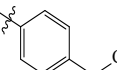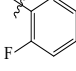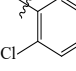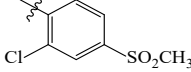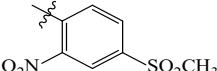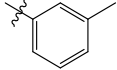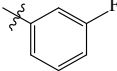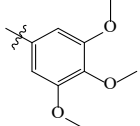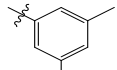
| Comp. | Ar | IC$_{50}$ (μM) | pIC$_{50}$ | |
		Obsd.	Obsd.	Pred.
ZD-1		1.247	5.904	5.840
ZD-2 *		1.276	5.894	5.877
ZD-3		1.365	5.865	5.860
ZD-4		0.998	6.001	5.997
ZD-5		1.324	5.878	5.879
ZD-6		5.000	5.301	5.402
ZD-7		3.475	5.459	5.470
ZD-8 *		0.283	6.548	6.528
ZD-9		0.261	6.583	6.579
ZD-10		1.503	5.823	5.781
ZD-11		1.346	5.871	5.903
ZD-12 *		0.352	6.454	6.471
ZD-13		1.457	5.845	5.839

Table 7. *Cont.*
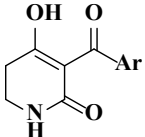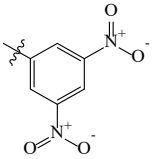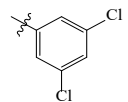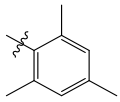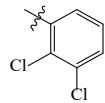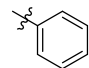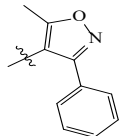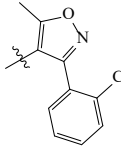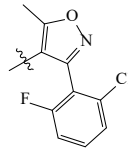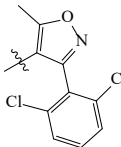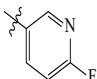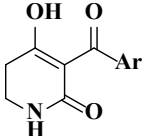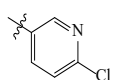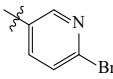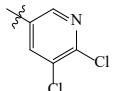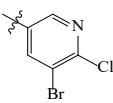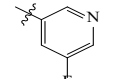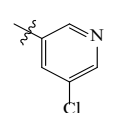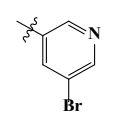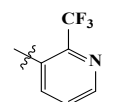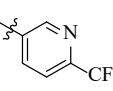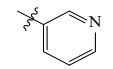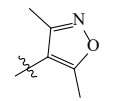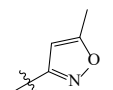
Comp.	Ar	IC$_{50}$ (μM)	pIC$_{50}$	
		Obsd.	Obsd.	Pred.
ZD-14		1.203	5.938	5.890
ZD-15		0.268	6.572	6.588
ZD-16 *		2.075	5.683	5.750
ZD-17		0.561	6.251	6.205
ZD-18		4.446	5.352	5.341
ZD-19		3.327	5.478	5.480
ZD-20		3.206	5.494	5.541
ZD-21 *		2.506	5.601	5.576
ZD-22		3.076	5.512	5.533
ZD-23		1.321	5.879	5.880

Table 7. *Cont.*

Comp.	Ar	IC$_{50}$ (μM)	pIC$_{50}$	
		Obsd.	Obsd.	Pred.
ZD-24		1.202	5.920	5.930
ZD-25		1.138	5.944	5.960
ZD-26		0.998	6.001	6.082
ZD-27		0.425	6.372	6.333
ZD-28		1.782	5.749	5.891
ZD-29 *		1.589	5.799	5.888
ZD-30		1.347	5.868	5.911
ZD-31		2.238	5.676	5.590
ZD-32		1.419	5.848	5.838
ZD-33 *		7.656	5.116	5.140
ZD-34		4.256	5.371	5.380
ZD-35		4.009	5.397	5.361

* Compounds were considered as the test set. IC$_{50}$: Half maximal inhibitory concentration toward *At*HPPD.

3.2. Topomer CoMFA Modeling Construction and Virtual Screening

The template compound ZD-9 was split into two R-groups (Figure 11). Other compounds in the training set were dissected automatically in ZD-9 segmentation manner.

Unrecognized molecules needed to be cut manually. After cutting, the fragment conformation was adjusted according to empirical rules to generate the Topomer CoMFA model.
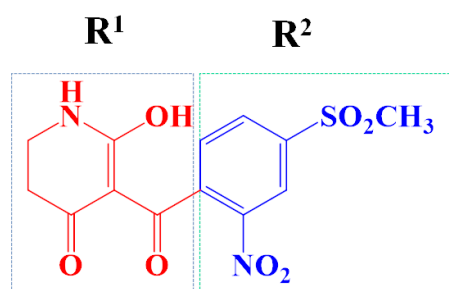
Figure 11. Splitting scheme used to define the two fragments (R^1—red and R^2—blue) for developing Topomer CoMFA model of HPPD inhibitors.

Highly active R-groups were screened from the Bailingwei (2012) database (approximately 50,000 fragments) using Topomer Search. Topomer Search-Details of Distance (TOPDIST) was selected at 185 to identify the degree of binding. Twenty-two novel pyridine derivatives were obtained, and their activities were predicted by the established Topomer CoMFA model.

3.3. Molecular Docking

Molecular docking studies were performed using CDOCKER of Discovery Studio (DS) (Biovia Inc., San Diego, CA, USA, 2020). The pose cluster radius was set to 0.5 in this program to ensure that docking ideas were as diverse as possible. The complex structure of HPPD (PDB ID: 6JX9) was obtained from the RCSB protein database [42]. Co-crystalline Y17107 was extracted from the enzyme structure, hydrogen was added, and all the heteroatoms and water molecules were removed. After replenishing all the missing amino acids, the structure of HPPD was protonated by the CHARMm force field, and all amino acid side chains were optimized.

3.4. ADMET Prediction

The top 22 compounds for the molecular docking score were predicted in terms of absorption, distribution, metabolism, excretion and toxicity (ADMET) with DS. Four pharmacokinetic parameters were calculated, including water solubility, cytochrome P450 (CYP450) binding and hepatotoxicity [43]. Five parameters were selected for toxicity prediction: oxygen biodegradability, carcinogenicity, ames mutagenicity, developmental toxicity potential and skin irritation screening.

3.5. MD Simulation

To predict the stability of HPPD protein binding to inhibitors, Amber 16 software was selected for the MD simulation. The side chain models of the cobalt coordination spheres of His308, His226 and Glu394 were used to create a builder module in the center of the metal by selecting the ff14SB field. The resulting structures were immersed in TIP3P water at a distance of 10 Å around the complexes, and an appropriate amount of counter ions were appended to the system to neutralize charges. The minimum process used a 2500-step conjugate gradient and 2500-step maximum descent algorithm. The system was gradually heated to 298 K by an isovolumic-isothermal, and equilibrium was achieved by simulating 1 ns in the isobaric-isothermal ensemble simulation. Finally, each system executed the PMEMD program unconstrained in the NTP integration for 50 ns with a time step of 2 fs. The root mean square deviation (RMSD) was used to evaluate the stability of the system.

3.6. AILDE and Physicochemical Properties

AILDE automatically performs calculations of substitution, energy minimization, and binding affinity assessments. All hydrogen was removed from the docking ligand-protein

complex, and the compound was submitted to the online server. The physicochemical properties of molecules were calculated by the "Small Molecules" of DS. The following parameters were predicted in the 2D topology descriptor: Log *p*, p*K*a, molecular weight (M_W), hydrogen bond acceptors (HBAs), hydrogen bond donors (HBDs), aromatic bonds (ARs) and surface area (SA). The electronegativity of the compounds was calculated using the "Connolly" of Gasteiger–Huckel of SYBYL software.

4. Conclusions

In this study, a reliable Topomer CoMFA model was established based on 35 pyridine HPPD inhibition herbicides. Twenty-two new compounds were designed via Topomer search according to the Topomer CoMFA model. The molecular docking results indicated that the ligands formed hydrogen bonds with Ser267 and π-π interactions with Phe381 and Phe424 at the active site. The 22 newly designed compounds were filtered through ADMET prediction, and finally, 9 compounds were obtained. MD simulations confirmed that Compounds Y12 and Y14 bear potential HPPD inhibition. Y12 was submitted to the AILDE platform, and 5 potential inhibitors were found in the activity-improved matrix. The established screening procedure is of great significance for the design of novel HPPD based herbicides.

Author Contributions: Y.F. and F.Y. conceived and designed the experiment and conveyed the manuscript information as corresponding authors. J.S. and S.G. repeated the experiment multiple times and then used it as an in-depth research content. J.S. designed and wrote the manuscript. J.-Y.W. and T.Y. carried out the methodology, calculation and writing the original draft. M.-L.Y. finished the visualization and investigation work. All authors have read and agreed to the published version of the manuscript.

Institutional Review Board Statement: Not applicable.

Informed Consent Statement: Not applicable.

Conflicts of Interest: The authors declare no conflict of interest.

References

1. Ahrens, H.; Lange, G.; Muller, T.; Rosinger, C.; Willms, L.; van Almsick, A. 4-Hydroxyphenylpyruvate dioxygenase inhibitors in combination with safeners: Solutions for modern and sustainable agriculture. *Angew. Chem. Int. Ed. Engl.* **2014**, *52*, 9388–9398. [CrossRef]
2. He, B.; Wang, D.W.; Yang, W.C.; Chen, Q.; Yang, G.F. Advances in research on 4-hydroxyphenylpyruvate dioxygenase (HPPD) structure and pyrazole-containing herbicides. *Chin. J. Org. Chem.* **2017**, *37*, 2895–2904. [CrossRef]
3. Li, H.B.; Li, L.; Li, J.X.; Han, T.F.; He, J.L.; Zhu, Y.Q. Novel HPPD inhibitors: Triketone 2H-benzo[b] [1,4] oxazin-3(4H)-one analogs. *Pest Manag. Sci.* **2018**, *74*, 579–589. [CrossRef] [PubMed]
4. Fu, Y.; Zhang, S.Q.; Liu, Y.X.; Wang, J.Y.; Gao, S.; Zhao, L.X.; Ye, F. Design, synthesis, SAR and molecular docking of novel green niacin-triketone HPPD inhibitor. *Ind. Crops Prod.* **2019**, *137*, 566–575. [CrossRef]
5. Fu, Y.; Zhang, D.; Zhang, S.Q.; Liu, Y.X.; Guo, Y.Y.; Wang, M.X.; Gao, S.; Zhao, L.X.; Ye, F. Discovery of n-aroyl diketone/triketone derivatives as novel 4-hydroxyphenylpyruvatedioxygenase inhibiting based herbicide. *J. Agric. Food Chem.* **2019**, *67*, 11839–11847. [CrossRef]
6. Neidig, M.L.; Kavana, M.; Moran, G.R.; Solomon, E.I. CD and MCD studies of the non-heme ferrous active site in (4-hydroxyphenyl) pyruvate dioxygenase: Correlation between oxygen activation in the extradiol and alpha-dependent dioxygenases. *J. Am. Chem. Soc.* **2004**, *126*, 4486–4487. [CrossRef]
7. Cho, J.E.; Kim, J.T.; Kim, E.; Ko, Y.K.; Kang, N.S. The structure-based three-dimensional pharmacophore models for arabidopsis thaliana HPPD inhibitors as herbicide. *Bull. Korean Chem. Soc.* **2013**, *34*, 2909–2914. [CrossRef]
8. Ndikuryayo, F.; Moosavi, B.; Yang, W.C.; Yang, G.F. 4-Hydroxyphenylpyruvate dioxygenase inhibitors: From chemical biology to agrochemicals. *J. Agric. Food Chem.* **2017**, *65*, 8523–8537. [CrossRef]
9. Zhang, F.W.; Qiao, Z.H.; Yao, C.T.; Sun, S.; Liu, W.T.; Wang, J.X. Effects of the novel HPPD-inhibitor herbicide QYM201 on enzyme activity and microorganisms, and its degradation in soil. *Ecotoxicology* **2021**, *30*, 80–90. [CrossRef]

10. Hu, W.; Gao, S.; Zhao, L.X.; Guo, K.L.; Wang, J.Y.; Gao, Y.C.; Shao, X.X.; Fu, Y.; Ye, F. Design, synthesis and biological activity of novel triketone-containing quinoxaline as HPPD inhibitor. *Pest Manag. Sci.* **2022**, *78*, 938–946. [CrossRef]

11. Wang, X.N.; Lin, H.Y.; Liu, J.J.; Zhao, X.Y.; Chen, X.; Yang, W.C.; Yang, G.F.; Zhan, C.G. The structure of 4-hydroxylphenylpyruvate dioxygenase complexed with 4-hydroxylphenylpyruvic acid reveals an unexpected inhibition mechanism. *Chin. Chem. Lett.* **2021**, *32*, 1920–1924. [CrossRef]

12. Santucci, A.; Bernardini, G.; Braconi, D.; Petricci, E.; Manetti, F. 4 Hydroxyphenylpyruvate dioxygenase and its inhibition in plants and animals: Small molecules as herbicides and agents for the treatment of human inherited diseases. *J. Med. Chem.* **2017**, *60*, 4101–4125. [CrossRef] [PubMed]

13. Takano, H.K.; Ovejero, R.F.L.; Belchior, G.G.; Maymone, G.P.L.; Dayan, F.E. ACCase-inhibiting herbicides: Mechanism of action, resistance evolution and stewardship. *Plant Physiol. Biochem.* **2021**, *78*, 176–187. [CrossRef]

14. Wang, Z.W.; Zhao, L.X.; Ma, P.; Ye, T.; Fu, Y.; Ye, F. Fragments recombination, design, synthesis, safener activity and CoMFA model of novel substituted dichloroacetylphenyl sulfonamide derivatives. *Pest Manag. Sci.* **2021**, *77*, 1724–1738. [CrossRef] [PubMed]

15. Song, H.M.; Zhao, L.X.; Zhang, S.Q.; Ye, T.; Fu, Y.; Ye, F. Design, synthesis, structure-activity relationship, molecular docking and herbicidal evaluation of 2-cinnamoyl-3-hydroxycyclohex-2-en-1-one as novel 4-hydroxyphenylpyruvate dioxygenase inhibitors. *J. Agric. Food Chem.* **2021**, *69*, 12621–12633. [CrossRef]

16. Huang, D.D.; Liu, Y.L.; Shi, B.B.; Li, Y.T.; Wang, G.X.; Liang, G.Z. Comprehensive 3D-QSAR and binding mode of BACE-1 inhibitors using R-group search and molecular docking. *J. Mol. Graph. Model.* **2013**, *45*, 65–83. [CrossRef]

17. Gupta, P.; Roy, N.; Garg, P. Docking-based 3D-QSAR study of HIV-1 integrase inhibitors. *Eur. J. Med. Chem.* **2009**, *44*, 4276–4287. [CrossRef]

18. Chhatbar, D.M.; Chaube, U.J.; Vyas, V.K.; Bhatt, H.G. CoMFA, CoMSIA, Topomer CoMFA, HQSAR, molecular docking and molecular dynamics simulations study of triazine morpholino derivatives as mTOR inhibitors for the treatment of breast cancer. *Comput. Biol. Chem.* **2019**, *80*, 351–363. [CrossRef]

19. Kang, T.; Gao, S.; Zhao, L.X.; Zhai, Y.; Ye, F.; Fu, Y. Design, synthesis and SAR of novel 1,3-disubstituted imidazolidine or hexahydropyrimidine derivatives as herbicide safeners. *J. Agric. Food Chem.* **2021**, *69*, 45–54. [CrossRef]

20. Wang, Z.; Cheng, L.P.; Kai, Z.P.; Wu, F.H.; Liu, Z.Y.; Cai, M.F. Molecular modeling studies of atorvastatin analogues as HMGR inhibitors using 3D-QSAR, molecular docking and molecular dynamics simulations. *Bioorg. Med. Chem. Lett.* **2014**, *24*, 3869–3876. [CrossRef]

21. Kristam, R.; Rao, S.N.; D'Cruz, A.S.; Mahadevan, V.; Viswanadhan, V.N. TRPV1 antagonism by piperazinyl-aryl compounds: A topomer-CoMFA study and its use in virtual screening for identification of novel antagonists. *J. Mol. Graph. Model.* **2017**, *72*, 112–128. [CrossRef] [PubMed]

22. Patel, A.; Bhatt, H.; Patel, B. Structural insights on 2-phenylquinazolin-4-one derivatives as tankyrase inhibitors through CoMFA, CoMSIA, topomer CoMFA and HQSAR studies. *J. Mol. Struct.* **2022**, *1249*, 131636. [CrossRef]

23. Tintori, C.; Magnani, M.; Schenone, S.; Botta, M. Docking, 3D-QSAR studies and in silico ADME prediction on c-Src tyrosine kinase inhibitors. *Eur. J. Med. Chem.* **2009**, *44*, 990–1000. [CrossRef] [PubMed]

24. Li, X.L.; Zhou, H.Y.; Mo, X.W.; Zhang, L.; Li, J. In silico study of febuxostat analogs as inhibitors of xanthine oxidoreductase: A combined 3D-QSAR and molecular docking study. *J. Mol. Struct.* **2019**, *1181*, 428–435. [CrossRef]

25. Tong, J.; Jiang, G.; Li, L.; Li, Y. Molecular virtual screening studies of herbicidal sulfonylurea analogues using molecular docking and topomer CoMFA research. *J. Struct. Chem.* **2019**, *60*, 210–218. [CrossRef]

26. Heravi, Y.E.; Sereshti, H.; Saboury, A.A.; Ghasemi, J.; Amirmostofian, M.; Supuran, C.T. 3D QSAR studies, pharmacophore modeling, and virtual screening of diarylpyrazole-benzenesulfonamide derivatives as a template to obtain new inhibitors, using human carbonic anhydrase II as a model protein. *J. Enzym. Inhib. Med. Chem.* **2017**, *32*, 688–700. [CrossRef]

27. Liu, Y.X.; Gao, S.; Ye, T.; Li, J.Z.; Ye, F.; Fu, Y. Combined 3D-quantitative structure–activity relationships and topomer technology-based molecular design of human 4-hydroxyphenylpyruvate dioxygenase inhibitors. *Future Med. Chem.* **2020**, *12*, 795–811. [CrossRef]

28. Tripathi, H.; Khan, F. Identification of potential inhibitors against nuclear dam1 complex subunit ask1 of Candida albicans using virtual screening and MD simulations. *Comput. Biol. Chem.* **2018**, *72*, 33–44. [CrossRef]

29. Hou, J.Y.; Zou, Q.; Wang, Y.J.; Gao, Q.; Yao, W.H.; Yao, Q.Z.; Zhang, J. Screening for the selective inhibitors of MMP-9 from natural products based on pharmacophore modeling and molecular docking in combination with bioassay experiment, hybrid QM/MM calculation, and MD simulation. *J. Biomol. Struct. Dyn.* **2019**, *37*, 3135–3149. [CrossRef]

30. Fu, Y.; Liu, Y.X.; Kang, T.; Sun, Y.N.; Li, J.Z.; Ye, F. Identifification of novel inhibitors of p-hydroxyphenylpyruvate dioxygenase using receptor-based virtual screening. *J. Taiwan Inst. Chem. Eng.* **2019**, *103*, 33–43. [CrossRef]

31. Jia, L.; Gao, S.; Zhang, Y.Y.; Zhao, L.X.; Fu, Y.; Ye, F. Fragmenlt recombination design, synthesis, and safener activity of novel ester-substituted pyrazole derivatives. *J. Agric. Food Chem.* **2021**, *69*, 8366–8379. [CrossRef] [PubMed]

32. Fatriansyah, J.F.; Rizqillah, R.K.; Yandi, M.Y.; Sahlan, M. Molecular docking and dynamics studies on propolis sulabiroin-A as a potential inhibitor of SARS-CoV-2. *J. King Saud Univ. Sci.* **2022**, *34*, 101707. [CrossRef]

33. Fu, Y.; Liu, Y.X.; Yi, K.H.; Li, M.Q.; Li, J.Z.; Ye, F. Quantitative structure activity relationship studies and molecular dynamics simulations of 2-(aryloxyacetyl)cyclohexane-1,3-diones derivatives as 4-hydroxyphenylpyruvate dioxygenase inhibitors. *Front Chem.* **2019**, *7*, 556. [CrossRef]

34. Brown, D.K.; Penkler, D.L.; Amamuddy, O.S.; Ross, C.; Atilgan, A.R.; Atilgan, C.; Bishop, O.T. MD-TASK: A software suite for analyzing molecular dynamics trajectories. *Struct. Bioinform.* **2017**, *33*, 2768–2771. [CrossRef] [PubMed]

35. Wei, F.J.; Kang, D.W.; Cherukupalli, S.; Zalloum, W.A.; Zhang, T.; Liu, X.Y.; Zhan, P. Discovery and optimizing polycyclic pyridone compounds as anti-HBV agents. *Expert Opin. Ther. Pat.* **2021**, *30*, 715–721. [CrossRef] [PubMed]

36. Edlin, C.D.; Morgans, G.; Winks, S.; Duffy, S.; Avery, V.M.; Wittlin, S.; Waterson, D.; Burrows, J.; Bryans, J. Identification and in-vitro ADME assessment of a series of novel anti-malarial agents suitable for hit-to-lead chemistry. *ACS Med. Chem. Lett.* **2012**, *3*, 570–573. [CrossRef] [PubMed]

37. Mei, L.; Wu, F.; Hao, G.F.; Yang, G.F. Protocol for hit-to-lead optimization of compounds by auto in silico ligand directing evolution (AILDE) approach. *STAR Protoc.* **2021**, *2*, 100312. [CrossRef]

38. Wu, F.X.; Zhuo, L.S.; Wang, F.; Huang, W.; Hao, G.F.; Yang, G.F. Auto in silico ligand directing evolution to facilitate the rapid and efficient discovery of drug lead. *iScience* **2020**, *23*, 101179. [CrossRef]

39. Tong, J.B.; Qin, S.S.; Lei, S.; Wang, Y. Molecular modeling studies of HIV-1 non-nucleoside reverse transcriptase inhibitors using 3D-QSAR, virtual screening, and docking simulations. *J. Serb. Chem. Soc.* **2019**, *84*, 303–316. [CrossRef]

40. Yu, S.L.; Zhou, Q.Q.; Zhang, X.L.; Jia, S.X.; Gan, Y.; Zhang, Y.H.; Shi, J.H.; Yuan, J.T. Hologram quantitative structure–activity relationship and topomer comparative molecular-field analysis to predict the affinities of azo dyes for cellulose fibers. *Dyes Pigm.* **2018**, *153*, 35–43. [CrossRef]

41. Tang, H.J.; Zhao, D.S. Studies of febuxostat analogues as xanthine oxidase inhibitors through 3D-QSAR, Topomer CoMFA and molecular modeling. *J. Iran. Chem. Soc.* **2019**, *16*, 2659–2671. [CrossRef]

42. He, B.; Dong, J.; Lin, H.Y.; Wang, M.Y.; Li, X.K.; Zheng, B.F.; Chen, Q.; Hao, G.F.; Yang, W.C.; Yang, G.F. Pyrazole-isoindoline-1,3-dione hybrid: A promising scaffold for 4-hydroxyphenylpyruvate dioxygenase inhibitors. *J. Agric. Food Chem.* **2019**, *67*, 10844–10852. [CrossRef] [PubMed]

43. Fu, Y.; Wang, M.; Zhao, L.X.; Zhang, S.Q.; Liu, Y.X.; Guo, Y.Y.; Zhang, D.; Gao, S.; Ye, F. Design, synthesis, herbicidal activity and CoMFA of aryl-formyl piperidinone HPPD inhibitors. *Pestic. Biochem. Physiol.* **2021**, *174*, 104811. [CrossRef]

44. Emanuela, G.; John, G.M.; David, T.M. Theoretical hydrogen bonding parameters for drug design. *J. Mol. Graph. Model.* **2001**, *19*, 349–362.

45. Zhu, T.; Jiao, Y.; Chen, Y.D.; Wang, X.; Li, H.F.; Zhang, L.Y.; Lu, T. Pharmacophore identification of Raf-1 kinase inhibitors. *Bioorg. Med. Chem. Lett.* **2008**, *18*, 2346–2350. [CrossRef]

46. Ferreira, L.L.G.; Andricopulo, A.D. ADMET modeling approaches in drug discovery. *Drug Discov. Today* **2019**, *24*, 1157–1165. [CrossRef]